Updated Lagrangian Taylor-SPH method
for elastic dynamic problems

H. Karim Serroukh^{a,*}, M. Mabssout^a

^{a}*Faculty of Science and Technology, Laboratory of Mechanics and Civil Engineering, Tangier, Morocco*

Abstract

This paper presents a discussion on the properties of the collocation meshfree method, the Updated Lagrangian Taylor-SPH (UL-TSPH), for dynamic problems in solid mechanics. The PDEs are written in mixed form in terms of stress and velocity for the elastodynamics problems. Two sets of particles are used to discretize the partial differential equations, resulting on avoiding the tensile instability inherent to classical SPH formulations. Numerical examples ranging from propagation of a shock wave in an elastic bar to a stationary Mode-I semi-Infinite cracked plate subjected to uniaxial tension are used to assess the performance of the proposed method.
© 2022 University of West Bohemia.

Keywords: meshfree method, Taylor-SPH, Updated Lagrangian, dynamic stress intensity factors

1. Introduction

The Finite Element Method (FEM) is the most popular mesh-based method used in computation solid mechanics, and many references can be found in the literature. Although the FEM has proved successful in modelling a range of problems, FEM has still a few drawbacks for modelling large deformations problems, presence the discontinuities and dynamic fracture.

To overcome the difficulties encountered by FEM in large deformation and problems involving discontinuities, several meshfree methods have been developed in the past being used in computational solid mechanics with a great success. In contrast to FEM, meshfree methods do not require a mesh connectivity procedure and they can perform numerical solutions without using a computational mesh-grid since they are based only on particles where field variables and their derivatives are estimated. Therefore, meshfree methods can deal in a simple manner with failure problems and large deformation without the problems encountered in mesh-based methods where mesh refinement is usually required.

Generally, meshfree methods are formulated using either the Galerkin meshfree methods based on the weak formulation of the PDEs or the collocation meshfree methods based on the strong formulation of the PDEs.

Galerkin meshfree methods require a special technique to implement the essential boundary conditions and the selection of a suitable numerical integration scheme, while the collocation meshfree methods are based on the strong form of the PDEs which leads to efficient formulations without numerical integration and essential boundary condition procedures.

A wide variety of meshfree methods have been proposed over the past years including the Element Free Galerkin Method [3], Reproducing Kernel particle Method (RKPM) [14], Smoothed Particle Hydrodynamics (SPH) developed by Lucy [17] and Gingold and Monaghan [8]

---

*Corresponding author. E-mail: hamza.karim.serroukh@gmail.com.

and the Taylor-SPH (TSPH) method developed by Herreros and Mabssout [9, 11, 18, 19]. The SPH method has been extended to problems involving fluid-structure interaction [1, 12]. In this paper, we will use the TSPH method, which has been successfully applied to solve linear and nonlinear problems [9, 11, 18, 19].

Generally, the SPH method suffers from two principal problems: (i) the lack of consistency on the boundary that can lead to poor accuracy. Various corrections have been developed to improve the precision of the SPH method and to restore the zeroth and first order completeness of the kernel function [2, 4, 10, 13, 16, 21] and (ii) tensile instability which appears in dynamic problems with material strength as reported by Swegle et al. [23]. To eliminate SPH tensile instabilities, Dyka et al. [5, 6] proposed a stress point approach where the unknowns such as density, stress and energy are estimated at some prescribed stress points placed among the SPH particles. This approach was later extended to two dimensions by Randles et al. [22].

Taylor-SPH (TSPH) meshfree method developed by the authors over the past years [9, 11, 18, 19] has been demonstrated to exhibit a good performance when applied to dynamic problems. The TSPH is a collocation meshfree method where the system of equations is written as a set of first-order hyperbolic partial differential equations. The method firstly consists a time discretization by mean of a Taylor series expansion in two steps and thereafter the space discretization using a corrected form of the SPH method. To solve the tensile instability, two different set of particles are used during simulation. It is worth mentioning that the classical SPH methods are written in simple terms of displacements and therefore Dirichlet boundary conditions for displacements and natural boundary conditions for traction must be considered. However, when using the TSPH meshfree method, the PDEs are formulated in mixed terms of stress and velocity, and thus only Dirichlet boundary conditions must be taken into account and are enforced in a simple manner at each particle on the border.

In previous works, the authors have extended the TSPH to large deformation problems [11]. The governing equation are written using the updated Lagrangian formulation. It was shown that the updated Lagrangian Taylor-SPH (UL-TSPH) produces very accurate results for solid mechanics involving large deformations and dynamic fracture. In this paper, the UL-TSPH is presented and it is applied to the propagation of the shock wave, to the vibration of a bar and to the elastodynamics crack problems, showing that the proposed numerical method is able to compute the Dynamic Intensity Factors and therefore it opens a new way to simulate dynamic fracture of a cracked material.

The paper is organized as follows. The partial differential equations using the Updated Lagrangian description are presented in Section 2. In Section 3, the PDEs are discretized using the UL-TSPH method. To show the performance of the proposed method, some numerical examples are presented in Section 4.

2. Mathematical model

The governing equations used in this work consists of (i) the momentum balance equations and (ii) a constitutive law defining the solid behavior. Here, we have restricted our analysis to an elastic material. In order to get an objective rate of the stress tensor, the Jaumann rate of the Cauchy stress is used. In terms of stress and velocity and neglecting the body forces, the governing equations are given by

$$\frac{\partial \boldsymbol{v}}{\partial t} = \frac{1}{\rho} \boldsymbol{\nabla} \boldsymbol{\sigma}, \tag{1}$$

$$\frac{\partial \boldsymbol{\sigma}}{\partial t} = \boldsymbol{D}^e : \boldsymbol{d} - \boldsymbol{S} \tag{2}$$

with

$$S = (\boldsymbol{\sigma}\omega - \omega\sigma),$$

where ρ is the material density, $\boldsymbol{\sigma}$ is the Cauchy stress tensor, $\boldsymbol{v}$ is the velocity vector, $\boldsymbol{d}$ is the rate of deformation tensor, $\boldsymbol{\omega}$ is the spin tensor and $\boldsymbol{D^e}$ is the elastic tensor. The term $\boldsymbol{S}$ in (2) come from the Jaumann rate of the Cauchy stress, where $\boldsymbol{\omega}$ is given by the antisymmetric part of the velocity gradient

$$\boldsymbol{\omega} = \frac{1}{2}(\boldsymbol{\nabla} \otimes \boldsymbol{v} - (\boldsymbol{\nabla} \otimes \boldsymbol{v})^T), \tag{3}$$

or

$$\omega_{ij} = \frac{1}{2}\left(\frac{\partial v_i}{\partial x_j} - \frac{\partial v_j}{\partial x_i}\right), \tag{4}$$

and $\boldsymbol{d}$ is given by the symmetric part of the velocity gradient

$$\boldsymbol{d} = \frac{1}{2}(\boldsymbol{\nabla} \otimes \boldsymbol{v} + (\boldsymbol{\nabla} \otimes \boldsymbol{v})^T), \tag{5}$$

or

$$d_{ij} = \frac{1}{2}\left(\frac{\partial v_i}{\partial x_j} + \frac{\partial v_j}{\partial x_i}\right). \tag{6}$$

Because the updated Lagrangian formulation is chosen here, the above equations are expressed in the current configuration which will be taken as the referential configuration.

In this paper, 2D plane stress problems are considered and therefore the stress and strain rate can be arranged in a matrix form as

$$\boldsymbol{\sigma} = (\sigma_{11}\ \sigma_{22}\ \sigma_{12})^T, \tag{7a}$$

$$\boldsymbol{d} = (d_{11}\ d_{22}\ 2d_{12})^T. \tag{7b}$$

3. Numerical model

The UL-TSPH method [11] is used to discretize (1) and (2). UL-TSPH consist of applying first the time discretization using a Taylor series expansion in two steps and thereafter the space discretization using a corrected form of the SPH method.

3.1. Time discretization

Time discretization of (1) and (2) are carried out using Taylor series expansion up to the second order of the unknowns $\boldsymbol{v}$ and stress $\boldsymbol{\sigma}$

$$\boldsymbol{v}^{n+1} = \boldsymbol{v}^n + \Delta t \frac{1}{\rho}\boldsymbol{\nabla} \cdot (\boldsymbol{\sigma})^n + \frac{\Delta t^2}{2}\frac{1}{\rho} \cdot \boldsymbol{\nabla}\left(\frac{\partial \boldsymbol{\sigma}}{\partial t}\right)^n + O(\Delta t^3), \tag{8}$$

$$\boldsymbol{\sigma}^{n+1} = \boldsymbol{\sigma}^n + \Delta t(\boldsymbol{D^e} : (\boldsymbol{d})^n - (\boldsymbol{S})^n) + \frac{\Delta t^2}{2}\boldsymbol{D^e} : \left(\frac{\partial \boldsymbol{d}}{\partial t}\right)^n - \frac{\Delta t^2}{2}\left(\frac{\partial \boldsymbol{S}}{\partial t}\right)^n + O(\Delta t^3). \tag{9}$$

To obtain the first order time derivatives of $\boldsymbol{S}, \boldsymbol{\sigma}$ and $\boldsymbol{d}$ in (8)–(9), we compute first the unknowns $\boldsymbol{\sigma}$ and $\boldsymbol{v}$ at an intermediate time $t^{n+\frac{1}{2}}$

$$\boldsymbol{v}^{n+\frac{1}{2}} = \boldsymbol{v}^n + \frac{\Delta t}{2}\frac{1}{\rho}\boldsymbol{\nabla} \cdot (\boldsymbol{\sigma})^n, \tag{10a}$$

$$\boldsymbol{\sigma}^{n+\frac{1}{2}} = \boldsymbol{\sigma}^n + \frac{\Delta t}{2}\boldsymbol{D^e} : (\boldsymbol{d})^n - \frac{\Delta t}{2}(\boldsymbol{S})^n. \tag{10b}$$

Therefore, the first-order time derivatives of $\boldsymbol{\sigma}$, $\boldsymbol{S}$ and $\boldsymbol{d}$ at time t^n are computed as follows:

$$\left(\frac{\partial \boldsymbol{\sigma}}{\partial t}\right)^n = \frac{2}{\Delta t}\left(\boldsymbol{\sigma}^{n+\frac{1}{2}} - \boldsymbol{\sigma}^n\right), \tag{11a}$$

$$\left(\frac{\partial \boldsymbol{S}}{\partial t}\right)^n = \frac{2}{\Delta t}\left(\boldsymbol{S}^{n+\frac{1}{2}} - \boldsymbol{S}^n\right), \tag{11b}$$

$$\left(\frac{\partial \boldsymbol{d}}{\partial t}\right)^n = \frac{2}{\Delta t}\left(\boldsymbol{d}^{n+\frac{1}{2}} - \boldsymbol{d}^n\right). \tag{11c}$$

Inserting (11) into (8) and (9), the unknowns $(\boldsymbol{\sigma}, \boldsymbol{v})$ at time t^{n+1} are computed as follows:

$$\boldsymbol{v}^{n+1} = \boldsymbol{v}^n + \Delta t\frac{1}{\rho}\boldsymbol{\nabla} \cdot (\boldsymbol{\sigma})^{n+\frac{1}{2}}, \tag{12a}$$

$$\boldsymbol{\sigma}^{n+1} = \boldsymbol{\sigma}^n + \Delta t\boldsymbol{D^e} : (\boldsymbol{d})^{n+\frac{1}{2}} - \Delta t(\boldsymbol{S})^{n+\frac{1}{2}}. \tag{12b}$$

The equations (10) and (12) represent the first and the second step, respectively, using UL-Taylor-SPH meshfree method.

3.2. Spatial discretization: Corrected SPH approximation

To perform the time discretization, the spatial discretization is required to obtain the numerical solution of the problem. A corrected form of SPH method is used to discretize (10) and (12) in space.

Here, a summary of the basic SPH method and its corrected form is presented in this section. SPH is based on the integral approximation of a given function $f(x)$ and its derivatives. The kernel approximation of function $f(x)$ by SPH is given by

$$\langle f(x)\rangle = \int_\Omega f(x')W(x - x', h)\,\mathrm{d}x', \tag{13}$$

where $W(x' - x, h)$ is the kernel function and h is the smoothing length defining the size of the kernel support.

The integral approximation of the gradient of a function $f(x)$ is given by

$$\langle \boldsymbol{\nabla} f(x)\rangle = -\int_\Omega f(x)\boldsymbol{\nabla} W(x - x', h)\,\mathrm{d}x', \tag{14}$$

where $\boldsymbol{\nabla} W(x - x', h)$ is the gradient of $W(x - x', h)$ with respect to x'.

The functions used as kernels in SPH approximations are required to fulfill some specific conditions [15]. They must be even function and must fulfill the following specific conditions:

$$\int_\Omega W(x - x', h)\,\mathrm{d}x' = 1, \tag{15a}$$

$$W(x - x', h) = 0 \text{ for } |x - x'| \geq kh, \tag{15b}$$

$$W(x - x', h) \geq 0, \tag{15c}$$

$$\lim_{h \to 0} W(x - x', h) = \delta(x - x'). \tag{15d}$$

In (15b), k is a positive parameter defining the smoothing support size of the kernel function.

In this work, the cubic spline function (16), proposed by Monaghan and Lattanzio [20], has been chosen as the kernel function

$$W(\xi, h) = C \begin{cases} \frac{2}{3} - \xi^2 + \frac{1}{2}\xi^3 & 0 \leq \xi \leq 1, \\ \frac{1}{6}(2 - \xi)^3 & 1 \leq \xi \leq 2, \\ 0 & \xi \geq 2, \end{cases} \tag{16}$$

with $\xi = \frac{|x-x'|}{h} = \frac{r}{h}$, the scaling factor C is given by $\frac{1}{h}$, $\frac{15}{7\pi h^2}$ and $\frac{3}{2\pi h^3}$ in 1D, 2D and 3D, respectively.

In the SPH method, a continuum is represented by a set of particles, thus the kernel integral (13) is approximated by a summation over a set of discretized particles

$$f_I = \sum_{J=1}^{N} f_J W_{IJ} \Omega_J, \tag{17}$$

where N is number of the neighboring particles of I such that $\|x_I - x_J\| \leq 2h$, f_I is the value of the function estimated at point I; $W_{IJ} = W(x_I - x_J, h)$ represents the value of the kernel function at position J and $\Omega_J = \frac{m_J}{\rho_J}$ is the volume related to particle J; m_J and ρ_J are the mass and density of particle J, respectively.

The particle approximation for the spatial derivative (14) is given by

$$\boldsymbol{\nabla} f_I = \sum_{J=1}^{N} \frac{m_J}{\rho_J} f_J \boldsymbol{\nabla} W_{IJ}, \tag{18a}$$

where

$$\boldsymbol{\nabla} W_{IJ} = \frac{x_{IJ}}{h \cdot r_{IJ}} \frac{\partial W_{IJ}}{\partial \xi}, \quad \xi = \frac{r_{IJ}}{h}, \quad r_{IJ} = |x_I - x_J|. \tag{18b}$$

SPH approximations (17) and (18) do not fulfill the consistency conditions for a given particle near to the boundary of the domain. The kernel function is truncated at the boundary. Therefore, the normality condition of the kernel function and its gradient is no longer valid. To restore the zeroth order and first order completeness conditions, a corrected form of the SPH meshfree method based on the normalization of the kernel function and its derivatives is used in this work.

Corrected form of the kernel approximation: In order to fulfill the C^0 consistency, the corrective kernel approximation for function $f(x_I)$ is given by [2, 4]

$$f_I = \sum_{J=1}^{N} f_J \tilde{W}_{IJ} \Omega_J, \tag{19a}$$

where

$$\tilde{W}_{IJ} = \frac{W_{IJ}}{\sum_{J=1}^{N} W_{IJ} \Omega_J}. \tag{19b}$$

The kernel approximation (19) represent constant functions and then it fulfills the C^0 consistency.

Corrected form of the first derivatives approximations: In order to fulfill the C^1 consistency, the corrected SPH approximation of the gradient of function f is given by [2, 4]

$$\boldsymbol{\nabla} f_I = \sum_{J=1}^{N} f_{IJ} \tilde{\boldsymbol{\nabla}} W_{IJ} \Omega_J, \tag{20a}$$

where

$$\tilde{\nabla} W_{IJ} = \frac{\boldsymbol{\nabla} w_{IJ}}{\left(\sum_{J=1}^{N} \boldsymbol{X}_{IJ} \otimes \boldsymbol{\nabla} W_{IJ} \Omega_J \right)} \tag{20b}$$

and

$$f_{IJ} = f_I - f_J. $$

SPH approximation (20) satisfies the zeroth and the first order derivative consistency; that is, the approximation of the zeroth and first order polynomials is exactly approximated.

3.3. Updated Lagrangian Taylor-SPH: Spatial discretization

As noted above, the time discretization is carried out in two steps using a Taylor series expansion. To perform this space discretization, the computational domain $\bar{\Omega} = \Omega \cup \partial\Omega$ is discretized in two set of particles: $\{x_k\}_1^{NR}$ real particles and $\{x_k\}_1^{NV}$ virtual particles where N_R and N_V denote real and virtual particles. The virtual particles will be interspersed among the real particles in a similar manner it was done in stress-point integration [6, 22] to stabilize the SPH method. Fig. 1 shows the distribution of real and virtual particles in 1D and 2D.
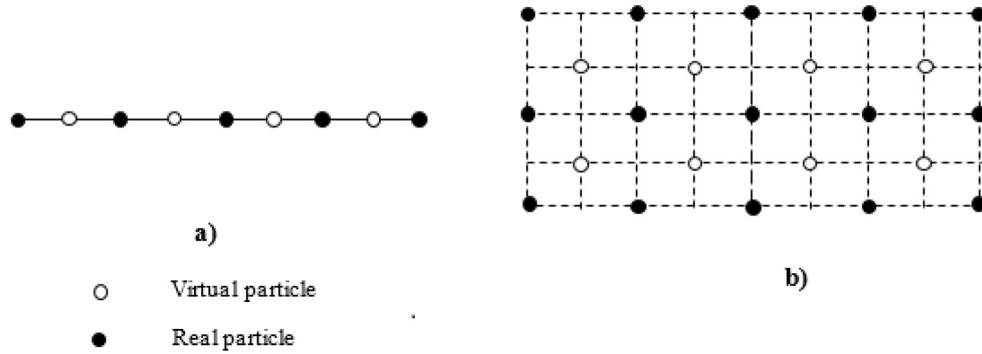

Fig. 1. Real and virtual particles arrangement: a) 1D and b) 2D problems

Using the UL-TSPH algorithm, the spatial discretization is carried out in two steps:

First step: Applying the corrected SPH spatial discretization (19) and (20) to the first-step time discretization (10), the unknown vectors $\boldsymbol{\sigma}_I^{n+\frac{1}{2}}$ and $\boldsymbol{v}_I^{n+\frac{1}{2}}$ for virtual particle I at time $t^{n+\frac{1}{2}}$ are obtained as

$$\langle \boldsymbol{\sigma}^{n+\frac{1}{2}} \rangle_I = \langle \boldsymbol{\sigma}^n \rangle_I + \frac{\Delta t}{2} \boldsymbol{D^e} : (\boldsymbol{d})_I^n + \frac{\Delta t}{2} (\boldsymbol{S})_I^n, \tag{21a}$$

$$\langle \boldsymbol{v}^{n+\frac{1}{2}} \rangle_I = \langle \boldsymbol{v}^n \rangle_I + \frac{\Delta t}{2} \frac{1}{\rho} \boldsymbol{\nabla} \cdot (\boldsymbol{\sigma})_I^n, \tag{21b}$$

$$\boldsymbol{\sigma}_I^{n+\frac{1}{2}} = \boldsymbol{\sigma}_I^n + \frac{\Delta t}{2} \left(\frac{1}{2} \boldsymbol{D^e} : \sum_{J=1}^{Nr} \frac{m_J}{\rho_J} (\boldsymbol{v}_J - \boldsymbol{v}_I)^n \check{\nabla} W_{IJ} + \sum_{J=1}^{Nr} \frac{m_J}{\rho_J} \boldsymbol{S}_J^n \check{W}_{IJ} \right), \tag{21c}$$

$$\boldsymbol{v}_I^{n+\frac{1}{2}} = \boldsymbol{v}_I^n + \frac{\Delta t}{2} \frac{1}{\rho} \left(\sum_{J=1}^{Nr} \frac{m_J}{\rho_J} (\boldsymbol{\sigma}_J - \boldsymbol{\sigma}_I)^n \check{\nabla} W_{IJ} \right). \tag{21d}$$

Second step: Applying the corrected SPH spatial discretization (19) and (20) to the second step time discretization (12), unknown vectors $\boldsymbol{\sigma}_I^{n+1}$ and $\boldsymbol{v}_I^{n+1}$ for real particles I at time t^{n+1}

are obtained as follows:

$$\langle \boldsymbol{\sigma}^{n+1} \rangle_I = \langle \boldsymbol{\sigma}^n \rangle_I + \Delta t \boldsymbol{D^e} : (\boldsymbol{d})_I^{n+\frac{1}{2}} + \Delta t (\boldsymbol{S})_I^{n+\frac{1}{2}}, \tag{22a}$$

$$\langle \boldsymbol{v}^{n+1} \rangle_I = \langle \boldsymbol{v}^n \rangle_I + \Delta t \frac{1}{\rho} \boldsymbol{\nabla} \cdot (\boldsymbol{\sigma})_I^{n+\frac{1}{2}}, \tag{22b}$$

$$\boldsymbol{\sigma}_I^{n+1} = \boldsymbol{\sigma}_I^n + \Delta t \left(\frac{1}{2} \boldsymbol{D^e} : \sum_{J=1}^{Nv} \frac{m_J}{\rho_J} (\boldsymbol{v}_J - \boldsymbol{v}_I)^{n+\frac{1}{2}} \check{\boldsymbol{\nabla}} W_{IJ} + \sum_{J=1}^{Nv} \frac{m_J}{\rho_J} \boldsymbol{S}_J^{n+\frac{1}{2}} \check{W}_{IJ} \right), \tag{22c}$$

$$\boldsymbol{v}_I^{n+1} = \boldsymbol{v}_I^n + \Delta t \frac{1}{\rho} \left(\sum_{J=1}^{Nr} \frac{m_J}{\rho_J} (\boldsymbol{\sigma}_J - \boldsymbol{\sigma}_I)^{n+\frac{1}{2}} \check{\boldsymbol{\nabla}} W_{IJ} \right). \tag{22d}$$

Finally, at the end of a certain time step, the positions of the real particles are updated

$$\boldsymbol{x}_I^{n+1} = \boldsymbol{x}_I^n + \Delta t \boldsymbol{v}_I^{n+\frac{1}{2}}, \tag{23}$$

where particle I refers to real particle.

The new position of the virtual particles is updated as the centroids of the Delaunay triangulation of the new real particles position.

4. Numerical examples

4.1. Propagation of a shock wave on a 1D elastic bar: Numerical stability

In this section, we analyze the influence of the smoothing length and the Courant number on the convergence of the UL-TSPH.

4.1.1. Sensitivity of the numerical results with respect to the smoothing length

It is well known that in the SPH method, the smoothing length h plays an important role since it has direct influence on the accuracy of the solution [18].

If h is too small, there may be not enough particles number in the smoothing support of dimension kh to interact with a given particle, which results in very low precision. By contrast, if h is too large, local properties perhaps smoothed out, and the precision decreases too. In order to perform a sensitivity testing of the UL-TSPH method with respect to the smoothing length h, the problem of the propagation of a shock wave in an elastic bar has been analyzed.

The initial and Dirichlet boundary conditions are as follows:

- Initial conditions

$$v(x,0) = \sigma(x,0) = 0, \quad 0 \le x \le L. \tag{24a}$$

- Boundary conditions: On $x = 0$:

$$v(0,t) = \begin{cases} 10 \text{ m/s} & \text{for } t \le 2.5 \text{ ms}, \\ 0 & \text{for } t > 2.5 \text{ ms}. \end{cases} \tag{24b}$$

On $x = L$:

$$v(L,t) = 0. \tag{24c}$$

The parameters and the material properties of the bar are taking as follows: elastic modulus $E = 80$ MPa, density $\rho = 2\,000$ kg/m^3 and length $L = 1$ m. The elastic wave speed is $c = \sqrt{\frac{E}{\rho}} = 200$ m/s.

There is an exact solution available for this problem. The incoming wave propagates towards the right boundary keeping its initial amplitude of $\sigma_0 = v_0\sqrt{E\rho} = 4$ MPa and $v_0 = 10$ m/s without any distortion and diffusion. It reflects at the fixed end ($L = 1$ m) at time $t_0 = \frac{L}{c} = 5$ ms and the stress is doubled to a value of 8 MPa, while the velocity of the wave after reflection propagates along the bar with $v_0 = -10$ m/s.

The bar has been discretized using 101 real particles and 100 virtual particles. The time step used for the computation $\Delta t = 5 \times 10^{-5}$ s which corresponds to the Courant number $C = \frac{c\Delta t}{\Delta x} = 1$. The smoothing length which determines the number of particles used in the computation can be written as

$$h = \alpha\Delta x. \tag{25}$$

Factor α defines the radius of the kernel function which relates the interparticle spacing to the smoothing length. For the cubic spline kernel, the smoothing domain has radius $2h$. The value of factor α has been gradually increased and the sensitivity of the numerical solution for different h has been studied. Factor α was given values of $\alpha = 1.2, 1.8$ and 2.2, corresponding to 5, 7 and 9 neighbor real particles inside the support domain.

Fig. 2 illustrates the stress $\sigma(L, t)$ for the three values of α. It can be observed that for $\alpha = 1.2$, the numerical solution converges well to the exact solution with an error about $2.5 \times 10^{-3}\%$. When α is increased ($\alpha = 1.8; 2.2$) the numerical oscillations appear; the error increases to 25% and the solution diverges. Using the L_2 norm, the error of the numerical method as function of factor α is given in Table 1.
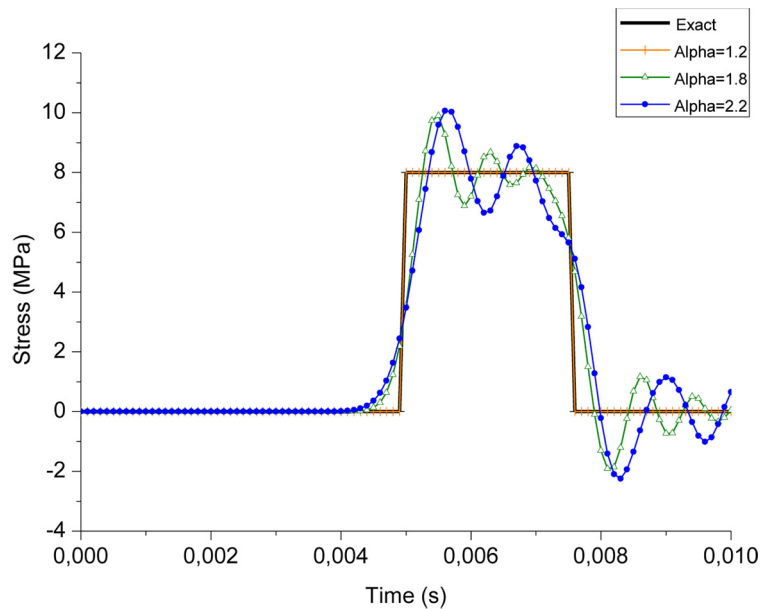

Fig. 2. Stress at the fixed end. Sensitivity of numerical solution with respect to the smoothing length

Table 1. Error L_2 for different values of factor α

Factor	Radius of compact support $r = 2h$ (m)	Number of particles inside the compact domain	Error L_2 (%)
1.2	0.024	4	2.5×10^{-5}
1.8	0.036	6	16.82
2.2	0.044	8	25.70

This example was calculated with a non-uniform particle distribution along the bar. Fig. 3 presents the stress history at point $x = 0.44$ m. As expected, the solution is stable but it exhibits small oscillations at discontinuities of the wave.
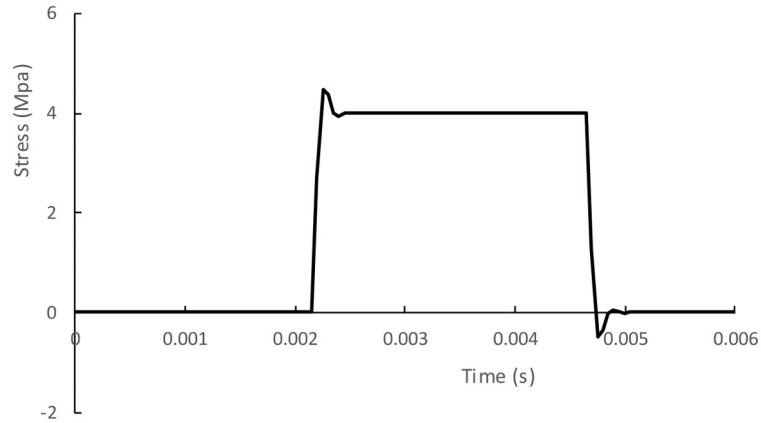

Fig. 3. Stress at $x = 0.44$ m for a non-uniform particle distribution

These oscillations are present where the distance between two consecutive particles is not constant and the local Courant number is not equal to 1. For complex geometries where a non-uniform particle distribution is required, a local maximum time step satisfying the CFL condition can be used. That allows to avoid the use of the smallest time step imposed by the smallest distance between two consecutive particles for the whole domain.

4.1.2. Sensitivity of the numerical results with respect to the Courant number

In order to accomplish a sensitivity analysis of the UL-TSPH with respect to the Courant number, a similar study as above has been carried using different values of C. The factor α is kept constant equal to 1.2 ($\alpha = 1.2$). The value of time step Δt has been gradually increased and the accuracy and stability of the numerical solution for different Courant number C have been tested.

Fig. 4 shows the stress $\sigma(L, t)$ for different Courant number after reflection of the wave using the proposed method. It can be observed that when the $C = 1$, the accuracy of the solution
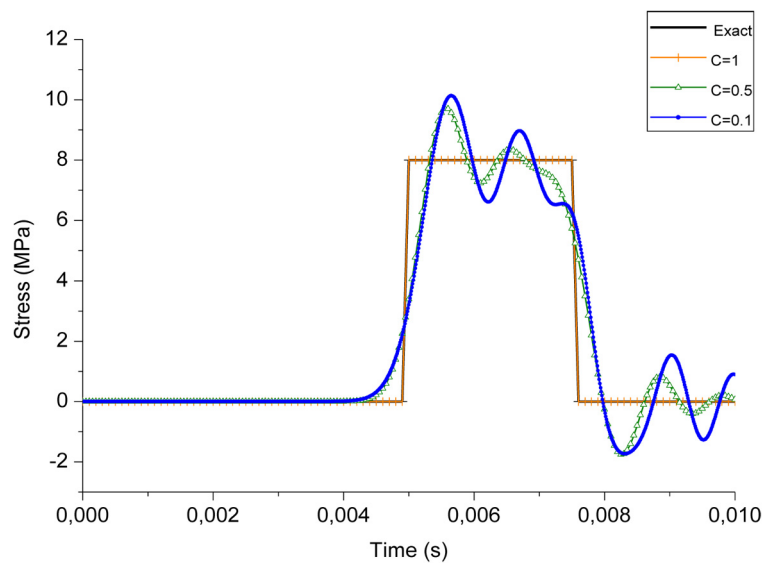

Fig. 4. Stress at the fixed end of the bar for different Courant number using UL-TSPH

gets its maximum, the error is about $2.5 \times 10^{-3}\%$. As can we see, the numerical results loses its accuracy when the Courant number is decreased and the solution becoming oscillatory. For $C > 1$, the numerical solution becomes unstable. The error using the L_2 norm is given in Table 2 for different Courant number.

Table 2. Error estimation for different values of the Courant number

δt (s)	Courant number	Error L_2 (%)
5×10^{-5}	1.0	2.5×10^{-5}
2.5×10^{-5}	0.5	17.44
5×10^{-6}	0.1	27.12
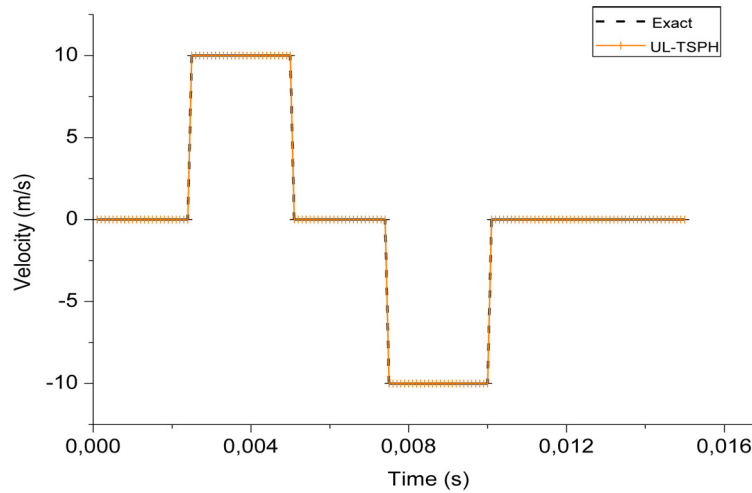
Fig. 5. Velocity at $x = 0.5$ m

Fig. 5 presents the velocity at the middle of the bar using UL-TSPH with $\alpha = 1.2$ and $C = 1$. As it can be observed, the numerical solution is free of dispersion and diffusion and the result is in complete agreement with the exact solution.

Fig. 6 gives time histories of kinetic energy, elastic strain energy and total energy obtained using the UL-TSPH method with $C = 1$. The proposed algorithm is shown to possess excellent energy conservation property.
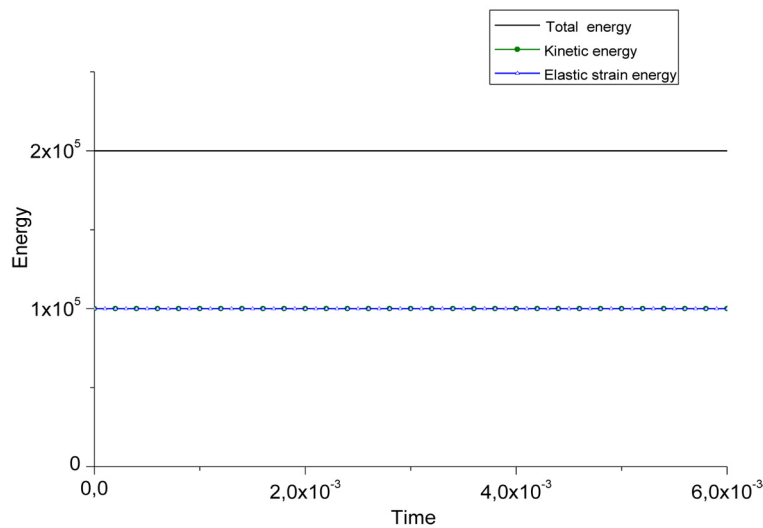

Fig. 6. Evolution of kinetic energy, elastic strain energy and total energy with $C = 1$

4.2. Vibration of a bar with fixed ends

To show the performance of the proposed method, we consider a vibrating elastic bar fixed at both ends as shown in Fig. 7 and the initial longitudinal velocity $v(x) = v_0 \sin\left(\frac{\pi x}{L}\right)$ is applied to the bar. The parameters and material properties are taking as follows: $v_0 = 0.1$ m/s, length $L = 1$ m, Elastic modulus $E = 50$ Pa and density $\rho = 25$ kg/m^3.
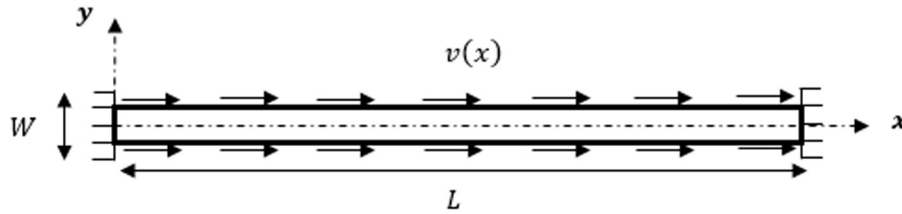

Fig. 7. Geometry of bar vibration

We have used 201 real particles for the simulation. To demonstrate the accuracy of the proposed algorithm, the results are compared with the analytical solution given in terms of displacement and stress as

$$u(x,t) = \frac{v_0 L}{\pi c} \sin\left(\frac{\pi c t}{L}\right) \sin\left(\frac{\pi x}{L}\right), \tag{26a}$$

$$\sigma(x,t) = E\frac{v_0}{c} \sin\left(\frac{\pi c t}{L}\right) \cos\left(\frac{\pi x}{L}\right), \tag{26b}$$

where $c = \sqrt{E/\rho} = \sqrt{2}$ m/s represents the elastic wave speed in the bar.

The Fig. 8 presents the stress and displacement along the x axis using the analytical solution and the UL-TSPH method at time $t = 0.353\,8$ s. The results are free of diffusion and dispersion and show an excellent agreement between the numerical and the exact solutions.

Fig. 9 shows the contour of stress along the bar at different time. The results are stable and free of oscillations.

In order to check the convergence of the method, this example has been calculated for three particles spacing: 0.02 m; 0.01 m; 5×10^{-3} m. The time step is kept constant equal to 3.53×10^{-3} s. Table 3 presents the L_2 error for each case, showing clearly the convergence of the proposed method with a small number of particles.

Table 3. L_2 error for different number of particles

Number of particles	CFL	L_2 error (%)
51	0.25	7.52
101	0.50	4.45
201	1.00	0.96

4.3. Stationary Mode-I semi-infinite crack

In this example, the dynamic stress intensity factors (DSIFs) for an infinite plate with a semi-infinite lateral crack is evaluated using UL-TSPH meshfree method. The plate loaded by uniform tensile stress perpendicular to the crack-face with the amplitude $\sigma_0 = 500$ MPa as shown in Fig. 10.
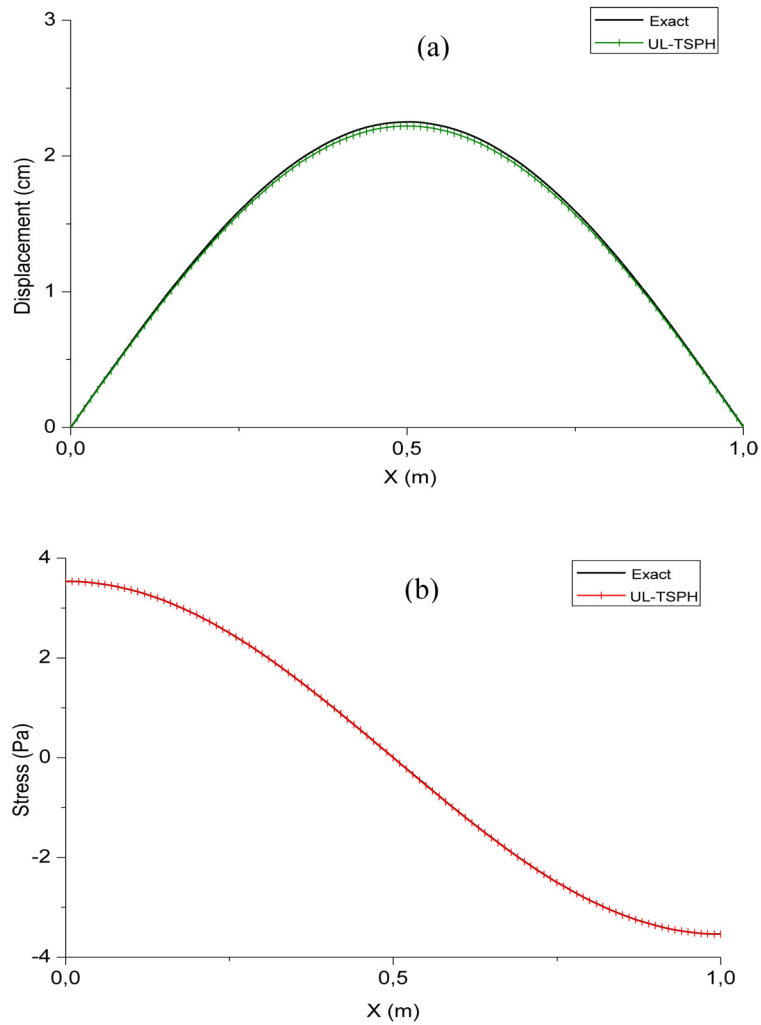
Fig. 8. Comparison between analytical and numerical solutions: (a) displacement, (b) stress

The applied boundary conditions are as follows:

(i) Γ_1 is fixed, $v_1 = v_2 = 0$,

(ii) on $\Gamma_2 \cup \Gamma_3$, $\sigma_{xy} = v_1 = 0$,

(iii) finally, stress at Γ_4 is $\sigma_{yy} = \sigma(t)$.

The plate dimensions are taken as follows: length $L = 10$ m, vertical half-height of the plate $H = 2$ m and crack length $a = 5$ m. The material properties are taken as: Young's modulus $E = 210$ GPa, Poisson ratio $\nu = 0.3$ and density $\rho = 8\,000$ kg.

The analytical solution is given by [7]

$$K_{dy}(0,t) = \begin{cases} 0 & \text{if } t < tc, \\ \frac{2\sigma_0}{1-\nu}\sqrt{\frac{c_d(t-tc)(1-2\nu)}{\pi}} & \text{if } t \geq tc, \end{cases} \tag{27a}$$

where t_c is the time needed by the stress wave to reach the crack-tip and given by

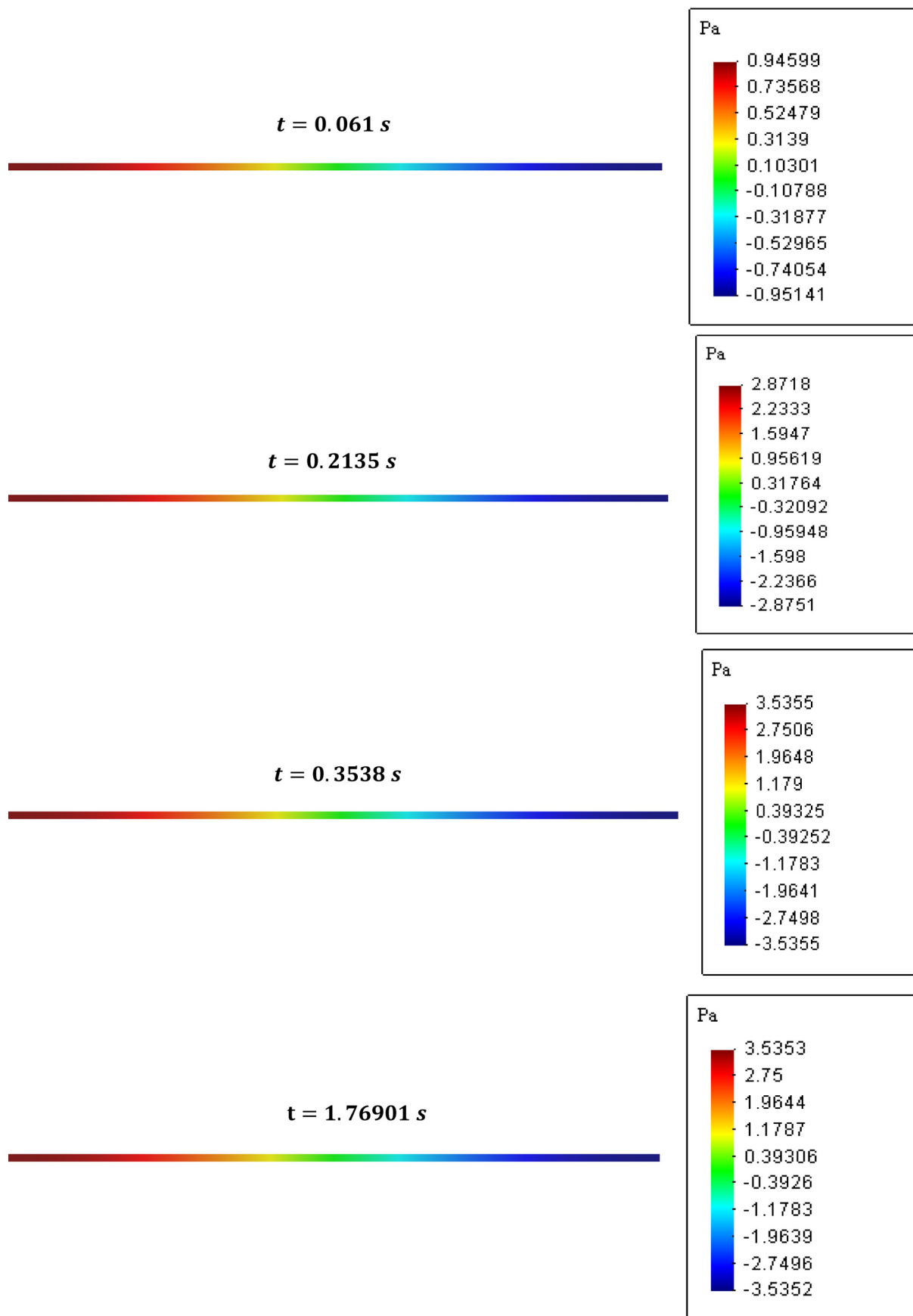$$t_c = H/c_d, \tag{27b}$$

where c_d is the dilatational wave speed.

$t = 0.061\ s$

Pa	
	0.94599
	0.73568
	0.52479
	0.3139
	0.10301
	-0.10788
	-0.31877
	-0.52965
	-0.74054
	-0.95141

$t = 0.2135\ s$

Pa	
	2.8718
	2.2333
	1.5947
	0.95619
	0.31764
	-0.32092
	-0.95948
	-1.598
	-2.2366
	-2.8751

$t = 0.3538\ s$

Pa	
	3.5355
	2.7506
	1.9648
	1.179
	0.39325
	-0.39252
	-1.1783
	-1.9641
	-2.7498
	-3.5355

t $= 1.76901\ s$

Pa	
	3.5353
	2.75
	1.9644
	1.1787
	0.39306
	-0.3926
	-1.1783
	-1.9639
	-2.7496
	-3.5352

Fig. 9. Distribution of stress σ_{xx} at different times
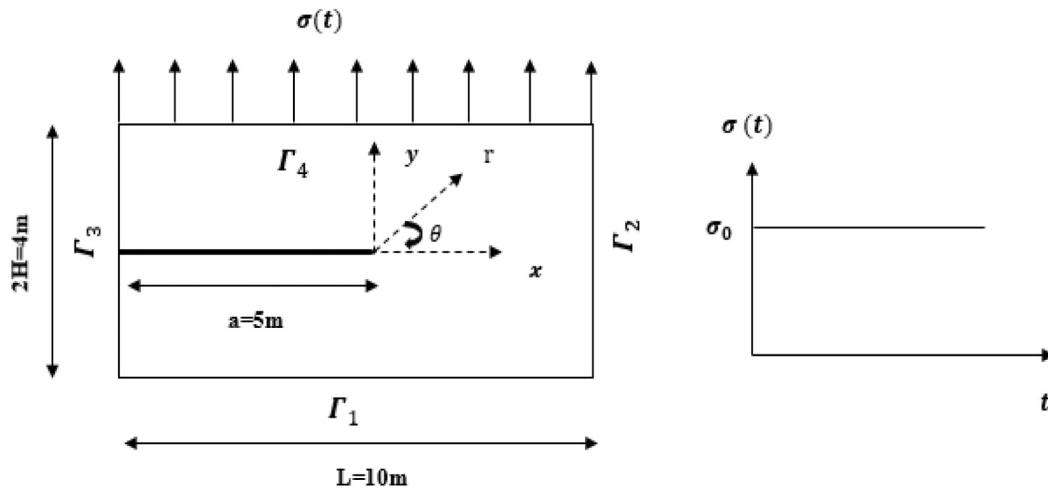
Fig. 10. Geometry and Heaviside step loading

The normalized DSIFs is given by

$$\tilde{K}_{dy} = K_{dy}(t)/\sigma_0\sqrt{H} \tag{28}$$

with

$$K_{dy}(t) = \sqrt{2\pi r}\,\sigma_{yy}(t), \tag{29}$$

where r represents the distance from the crack tip along the line $\theta = 0°$.

Fig. 11 presents the normalized DSIFs as a function of a normalized time obtained by using the UL-TSPH method. As can be seen, the numerical results converge well to the exact solution with 101×41 SPH particles.
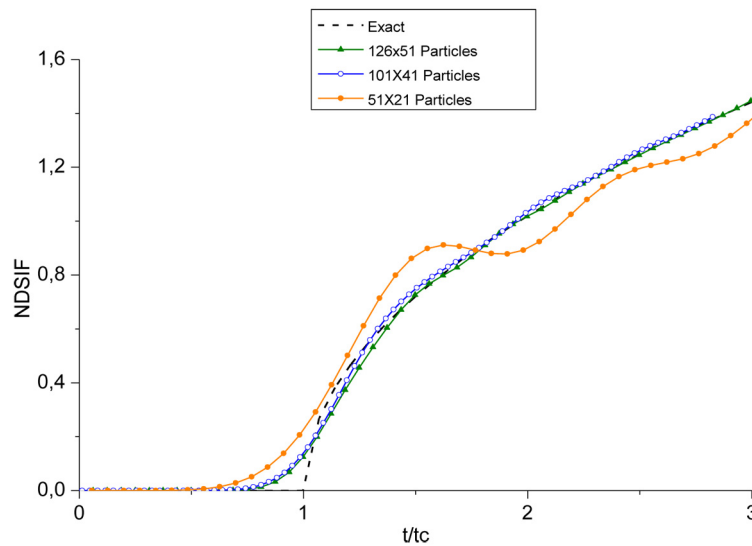

Fig. 11. Normalized mode-I DSIFs versus normalized time for different number of particles

5. Conclusion

A collocation meshfree method Updated Lagrangian-Taylor-SPH for large deformation in dynamic problems has been presented. The governing equations are written in mixed terms of stress and velocity. The time discretization is carried out using Taylor series expansion and the space discretization based on corrected form of SPH method.

From the examples presented in Section 4, the following can be deduced:

- The UL-TSPH presents good shock wave propagation properties minimizing numerical diffusion and dispersion.

- It avoids numerical instabilities in a natural manner.

- It is an efficient tool to assess the Dynamic Stress Intensity Factors. Therefore, it opens a new way to simulate dynamic fracture of a cracked material.

- The method is efficient, robust, easy to implement and only few particles are needed to get accurate results.

References

[1] Antoci, C., Gallati, M., Sibilla, S., Numerical simulation of fluid-structure interaction by SPH, Computers and Structures 85 (2007) 879–890. https://doi.org/10.1016/j.compstruc.2007.01.002

[2] Belytschko, T., Krongauz, Y., Dolbow, Y., Gerlach, C., On the completeness of meshfree particle methods, International Journal for Numerical Methods in Engineering 43 (1998) 785–819. https://doi.org/10.1002/(SICI)1097-0207(19981115)43:5<785::AID-NME420>3.0.CO;2-9

[3] Belytschko, T., Krongauz, Y., Organ, D., Fleming, M., Krysl, P., Meshless methods: An overview and recent developments, Computer Methods in Applied Mechanics and Engineering 139 (1996) 3–47. https://doi.org/10.1016/S0045-7825(96)01078-X

[4] Chen, J. K., Beraun, J. E., Carney, T. C., A corrective smoothed particle method for boundary value problems in heat conduction, International Journal for Numerical Methods in Engineering 46 (1999) 231–252.
https://doi.org/10.1002/(SICI)1097-0207(19990920)46:2<231::AID-NME672>3.0.CO;2-K

[5] Dyka, C. T., Ingel, R. P., An approach for tension instability in smoothed particle hydrodynamics (SPH), Computers & Structures 57 (4) (1995) 573–580.
https://doi.org/10.1016/0045-7949(95)00059-P

[6] Dyka, C. T., Randles, P. W., Ingel, R. P., Stress points for tension instability in SPH, International Journal for Numerical Methods in Engineering 40 (1997) 2325–2341.
https://doi.org/10.1002/(SICI)1097-0207(19970715)40:13<2325::AID-NME161>3.0.CO;2-8

[7] Freund, L. B., Dynamic fracture mechanics, Cambridge UK: Cambridge University Press, London, 1989.

[8] Gingold, R. A., Monaghan, J. J., Smoothed particles hydrodynamics: Theory and application to non-spherical stars, Monthly Notices of the Royal Astronomical Society 181 (1977) 375–389.
https://doi.org/10.1093/mnras/181.3.375

[9] Herreros, M. I., Mabssout, M., A two-steps time discretization scheme using the SPH method for shock wave propagation, Computer Methods in Applied Mechanics and Engineering 200 (2011) 1833–1845. https://doi.org/10.1016/j.cma.2011.02.006

[10] Johnson, G. R., Beissel, S. R., Normalized smoothing functions for SPH impact computations, International Journal for Numerical Methods in Engineering 39 (1996) 2725–2741.
https://doi.org/10.1002/(SICI)1097-0207(19960830)39:16<2725::AID-NME973>3.0.CO;2-9

[11] Karim Serroukh, H., Mabssout, M., Herreros, M. I., Updated Lagrangian Taylor-SPH method for large deformation in dynamic problems, Applied Mathematical Modelling 80 (2019) 238–256.
https://doi.org/10.1016/j.apm.2019.11.046

[12] Khayyer, A., Shimizu, Y., Gotoh, H., Nagashima, K., A coupled incompressible SPH-Hamiltonian SPH solver for hydroelastic FSI corresponding to composite structures, Applied Mathematical Modelling 94 (2021) 242–271. https://doi.org/10.1016/j.apm.2021.01.011

[13] Liu, W. K., Jun, S., Adee, J., Belytschko, T., Reproducing kernel particle method for structural dynamics, International Journal for Numerical Methods in Engineering 38 (1995) 1665–1679. https://doi.org/10.1002/nme.1620381005

[14] Liu, W. K., Jun, S., Zhang, Y. F., Reproducing kernel particle methods, International Journal for Numerical Methods in Fluids 20 (1995) 1081–1106. https://doi.org/10.1002/fld.1650200824

[15] Liu, G. R., Liu, M. B., Smoothed particle hydrodynamics: A meshfree particle method, World Scientific Publishing, Singapore, 2003. https://doi.org/10.1142/9789812564405

[16] Liu, M. B., Liu, G. R., Lam, K. Y., Constructing smoothing functions in smoothed particle hydrodynamics with applications, Journal of Computational and Applied Mathematics 155 (2003) 263–284. https://doi.org/10.1016/S0377-0427(02)00869-5

[17] Lucy, L. B., Numerical approach to testing of fission hypothesis, The Astronomical Journal 82 (1977) 1013–1024. https://doi.org/10.1086/112164

[18] Mabssout, M., Herreros, M. I., Runge-Kutta vs Taylor-SPH. Two time integration schemes for SPH with application to soil dynamics, Applied Mathematical Modelling 37 (5) (2013) 3541–3563. https://doi.org/10.1016/j.apm.2012.08.014

[19] Mabssout, M., Herreros, M. I., Idder, H., Predicting dynamic fracture in viscoplastic materials using Taylor-SPH, International Journal of Impact Engineering 87 (2016) 95–107. https://doi.org/10.1016/j.ijimpeng.2015.06.015

[20] Monaghan, J. J., Lattanzio, J. C., A refined particle method for astrophysical problems, Astronomy and Astrophysics 149 (1985) 135–143.

[21] Randles, P. W., Libersky, L. D., Smoothed particle hydrodynamics: Some recent improvements and applications, Computer Methods in Applied Mechanics and Engineering139 (1996) 375–408. https://doi.org/10.1016/S0045-7825(96)01090-0

[22] Randles, P. W., Libersky, L. D., Normalized SPH with stress points, International Journal for Numerical Methods in Engineering 48 (2000) 1445–1462. https://doi.org/10.1002/1097-0207(20000810)48:10<1445::AID-NME831>3.0.CO;2-9

[23] Swegle, J. W., Hicks, D. A., Attaway, S. W., Smoothed particle hydrodynamics stability analysis, Journal of Computational Physics 116 (1995) 123–134. https://doi.org/10.1006/jcph.1995.1010